THE JOURNAL OF PHYSICAL CHEMISTRY Letters

Letter

pubs.acs.org/JPCL

Charge- and Size-Selective Ion Sieving Through $Ti_3C_2T_x$ MXene Membranes

Chang E. Ren,[†] Kelsey B. Hatzell,[†] Mohamed Alhabeb,[†] Zheng Ling,[†] Khaled A. Mahmoud,*[,‡] and Yury Gogotsi*[,†]

[†]Department of Materials Science and Engineering and A. J. Drexel Nanomaterials Institute, Drexel University, Philadelphia, Pennsylvania 19104, United States

[‡]Qatar Environment and Energy Research Institute, P.O. Box 5825, Doha, Qatar

Supporting Information

ABSTRACT: Nanometer-thin sheets of 2D $Ti_3C_2T_x$ (MXene) have been assembled into freestanding or supported membranes for the charge- and size-selective rejection of ions and molecules. MXene membranes with controllable thicknesses ranging from hundreds of nanometers to several micrometers exhibited flexibility, high mechanical strength, hydrophilic surfaces, and electrical conductivity that render them promising for separation applications. Micrometer-thick MXene membranes demonstrated ultrafast water flux of 37.4 L/(Bar·h·m^2) and differential sieving of salts depending on both the hydration radius and charge of the ions. Cations with a larger charge and hydration radii smaller than the interlayer spacing of MXene (~6 Å) demonstrate an order of magnitude slower permeation compared to single-charged cations. Our findings may open a door for developing efficient and highly selective separation membranes from 2D carbides.

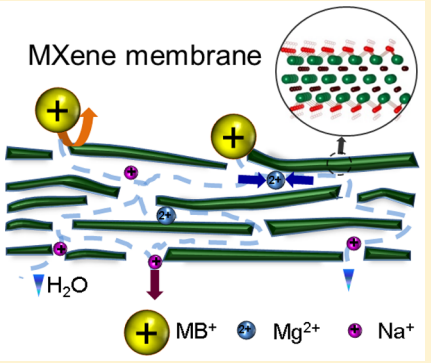

Recently, there have been significant efforts in preparing membranes from 2D materials, such as graphene[1] and graphene oxide (GO).[2−6] Joshi demonstrated that a 5 μm-thick GO membrane sieved inorganic salts and organic molecules with characteristic hydration radii above 4.5 Å.[5] Layered membranes are highly versatile as the ion rejection and water transport rate can be controlled by changing flake size, interlayer distance and overall membrane thickness.[3,7] However, there are not many 2D materials that can be processed into membranes that are able to selectively exclude ions based on size and charge, while maintaining mechanical integrity.

A new family of 2D materials based on transition metal carbides and/or nitrides, MXenes, have recently emerged and showed promising results in electrochemical energy storage applications, which utilize similar principles of controlled ion insertion between the atomically thin layers.[8−11] MXenes are produced by selectively etching monatomic A-element layers from the layered hexagonal transition metal carbides and/or nitrides, termed MAX phases[12] (Figure 1a). The most studied member of the MXene family is $Ti_3C_2T_x$, where T represents terminating functional groups (O, OH, and/or F), and x is the number of terminating groups. Similar to GO,[13] $Ti_3C_2T_x$ is characterized by a negative surface charge (zeta potential of as-produced $Ti_3C_2T_x$ solution is −39.5 mV,[14] and at pH 7 is −29 mV[15]) and hydrophilic surface with a contact angle around 25°,[11,14] which is a desirable property for ion separation in aqueous solutions. A 3.3-μm-thick $Ti_3C_2T_x$ film has a tensile strength of 22 MPa,[14] which is comparable to 55 MPa of a 2.5 μm-thick GO membrane.[16] Compared to insulating GO membranes, $Ti_3C_2T_x$ has a metallic conductivity (2400 S/cm[14]), which implies the potential to electrically modulate the surface charge and control ion permeation with an applied voltage. $Ti_3C_2T_x$ is an efficient adsorbent for the cationic dye

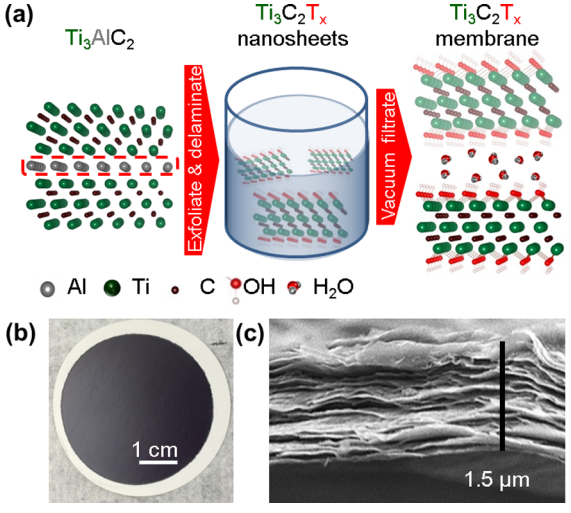

Figure 1. Preparation, structure, and images of $Ti_3C_2T_x$ membranes. (a) A schematic of the synthesis of a 2D $Ti_3C_2T_x$ membrane from Ti_3AlC_2. (b) Photograph and (c) cross-sectional SEM image of a $Ti_3C_2T_x$ membrane.

Received: August 28, 2015
Accepted: September 22, 2015
Published: September 22, 2015

DOI: 10.1021/acs.jpclett.5b01895
J. Phys. Chem. Lett. 2015, 6, 4026−4031

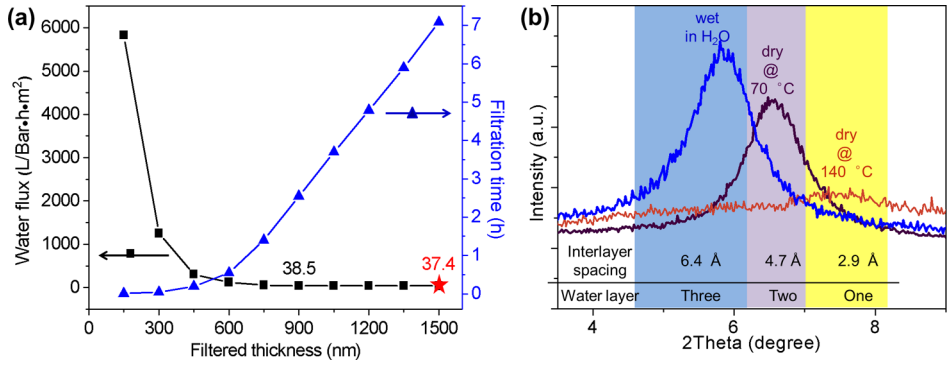

Figure 2. Water flux through $Ti_3C_2T_x$ membranes and water confinement between $Ti_3C_2T_x$ layers. (a) Water flux through $Ti_3C_2T_x$ membrane with varying thicknesses, and red star marks the thickness of membranes used in ion permeation tests. (b) (0002) peaks of XRD patterns of $Ti_3C_2T_x$ membranes at different moisture levels and average interlayer spacing calculated from XRD data.

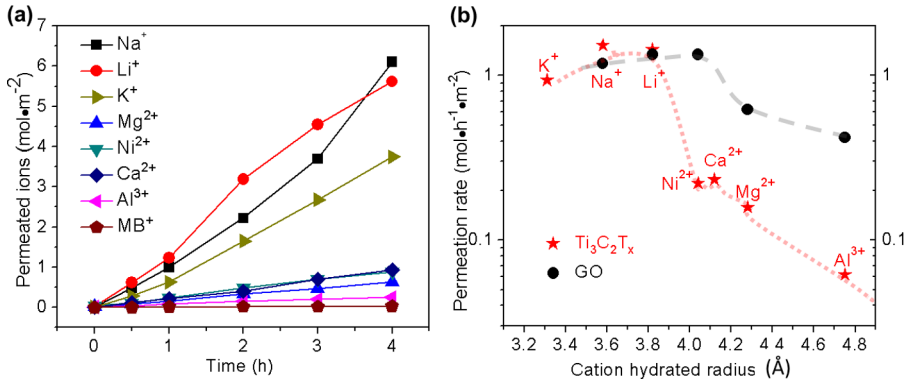

Figure 3. Cation permeation characteristics through $Ti_3C_2T_x$ and GO membranes. (a) Number of cations permeated through the $Ti_3C_2T_x$ membranes against time for 0.2 mol/L feed solutions (all solution utilize a Cl^- counteranions). (b) The permeation rates of cations against their hydration radii through the $Ti_3C_2T_x$ and GO membranes. The dashed curves are a guide to the eye.

methylene blue (MB),[17] gold,[18] lead (Pb^{2+})[19] and chromium (Cr^{6+}) cations.[15] Furthermore, it has been shown that a wide range of cations with varying sizes and charges (Na^+, K^+, NH_4^+, Mg^{2+} and Al^{3+}) can intercalate between $Ti_3C_2T_x$ layers,[9,20] and this process results in expansion or contraction of the films, dependent on the charge and nature of the cation.[21,22] However, ionic and water transport through MXene membranes of any kind has never been reported.

In this paper, we report the selective sieving of alkali, alkaline earth (Li^+, Na^+, K^+, Mg^{2+}, Ca^{2+}), transition and other metal (Ni^{2+} and Al^{3+}), and methylthioninium$^+$ (MB^+) dye cations through $Ti_3C_2T_x$ membranes. We compare $Ti_3C_2T_x$ and GO membranes under the same testing conditions (Experimental Methods and Figure SI1), and show that $Ti_3C_2T_x$ has a better selectivity toward metal cations of increasing charges than GO. Finally, based on the interlayer spacing of $Ti_3C_2T_x$ and mechanical deformation of $Ti_3C_2T_x$ upon intercalation, the mechanisms of ions transport through $Ti_3C_2T_x$ membranes are briefly discussed.

$Ti_3C_2T_x$ membranes were fabricated by a vacuum-assisted filtration (VAF) method, where colloidal solutions of delaminated $Ti_3C_2T_x$ (Supporting Information, Experimental Methods) were filtered to obtain membranes with controllable mass-loading and thickness. In order to obtain smooth membranes shown in Figure 1b,c and Figure SI2, dilute colloidal solution of $Ti_3C_2T_x$ (~0.01 mg/mL) was used.[23] It contained single-layer $Ti_3C_2T_x$ sheets with thickness of ~1 nm and lateral size on the order of hundreds of nanometers to several microns.[14] The high aspect ratio of single-layer $Ti_3C_2T_x$ ensures uniform and narrow 2D nanochannels and mitigates the presence of meso- and macro-pores across the membrane. Considering the relatively high pressure exerted on $Ti_3C_2T_x$ membranes during the experiments, commercial polyvinylidene fluoride (PVDF) supports (450 nm pores)[23] were used. PVDF membranes were tested alone and did not demonstrate any selectivity toward any molecule or ion in this study (Table SI1) and thus did not affect the $Ti_3C_2T_x$ membranes' performance.

By sequentially filtering dilute suspensions of $Ti_3C_2T_x$ of known concentrations (0.01 mg/mL), water flux was estimated from the filtration time and correlated with membrane thicknesses. An exponential decrease of water flux is observed initially for increasing membrane thicknesses and mass-loading (Figure 2a). When the membranes thickness was between 900 to 1500 nm, the water flux became constant ~38 L/(Bar·h·m^2). Permeation tests were conducted on membranes with the thicknesses of 1.5 ± 0.1 μm (Figure 1c) to ensure mechanical stability and the absence of pinholes. A water flux of 37.4 L/(Bar·h·m^2), compared to 6.5 L/(Bar·h·m^2) for a 1.5-μm-thick GO membrane tested in the same way, indicates ultrafast water permeation through $Ti_3C_2T_x$ membranes.

This fast water flow can be explained[35] by the presence of one or more layers of H_2O molecules between the $Ti_3C_2T_x$ layers in the wet state.[11,24] The hydration effect between $Ti_3C_2T_x$ layers was examined by studying three $Ti_3C_2T_x$ membranes at different moisture levels with X-ray diffraction (XRD) (Figure 2b). One sample was dried at 140 °C, another was dried at 70 °C, and the last sample was in a wet state. The XRD patterns of the membranes agreed well with previous

DOI: 10.1021/acs.jpclett.5b01895
J. Phys. Chem. Lett. 2015, 6, 4026−4031

Table 1. Permeation Rates of Cations from Chloride Solutions through the $Ti_3C_2T_x$ Membranes

ion	K^+	Na^+	Li^+	Ni^{2+}	Ca^{2+}	Mg^{2+}	Al^{3+}	MB^+
permeation rate, $mol \cdot h^{-1} \cdot m^{-2}$	0.94	1.53	1.40	0.22	0.23	0.16	0.06	7×10^{-4}

$Ti_3C_2T_x$ films,[14] and the FWHMs of the 140 °C-dried, 70 °C-dried and wet $Ti_3C_2T_x$ membranes were 1.72, 0.94 and 0.97°, respectively. The (0002) peak shifted to lower angles as the moisture increased, which corresponds to larger interlayer spacing between $Ti_3C_2T_x$ layers. The interlayer distances of the 140 °C-dried, 70 °C-dried, and wet $Ti_3C_2T_x$ membranes were calculated to be 2.9, 4.7, and 6.4 Å, corresponding to one, two and three layers of water molecules between $Ti_3C_2T_x$ layers, respectively.[5] The observed permeation rates for cations and dyes in our study are in agreement with a 2D nanochannel width around 6.4 Å.[5,16,25] Three water layers between $Ti_3C_2T_x$ sheets can create a free path for water flow and facilitate the high water flux observed before.[25]

The permeation rates of all solutions through $Ti_3C_2T_x$ and GO membranes were measured in a homemade U-shaped device (Figure SI1). One half of the cell was a chloride salt solution (0.2 mol/L), while the other half contained the same volume of deionized water. Both solutions were introduced at the same rate, and magnetic stirring was maintained on the permeate side to eliminate concentration gradients. The conductivity of the permeate side was measured over time to estimate concentration of ions and calculate ionic transport. All solutions utilized a salt with a Cl^- anion, and thus cation permeation rates were easily compared.

The pH of NaCl solution was stable around 6.05 throughout the test. This indicates that both Cl^- and Na^+ ions permeate through the $Ti_3C_2T_x$ membrane in stoichiometric quantities and that the number of permeated cations can be estimated from ionic conductivity measurements on the permeate side, as discussed in the Experimental Methods. The concentration of permeated cations shows a linear increase with time (Figure 3a), while the individual permeation rates (the slope of curves) decrease in the row $Na^+ > Li^+ > K^+ > Ca^{2+} > Ni^{2+} > Mg^{2+} > Al^{3+} \gg MB^+$. MB^+ demonstrated almost no permeation ($\sim 7 \times 10^{-4}$ $mol \cdot h^{-1} \cdot m^{-2}$), confirming that the $Ti_3C_2T_x$ membranes are free of pinholes.

The permeation rates through $Ti_3C_2T_x$ and GO membranes as a function of the cation size and charge are plotted in Figure 3b and listed in Table 1 and Table SI2. The effective volume occupied by a cation in water is characterized by its hydration radius.[26,27] Based on the permeation rates through $Ti_3C_2T_x$, all cations can be classified into four groups: (1) Na^+, Li^+ and K^+, (2) Ca^{2+}, Ni^{2+}, Mg^{2+}, (3) Al^{3+}, and (4) MB^+, suggesting the role of cations' size and charge. Na^+ has the highest permeation rate of 1.53 $mol \cdot h^{-1} \cdot m^{-2}$, which is about 25 times faster than Al^{3+}, and 7 times that of Ca^{2+} ion. Despite a smaller hydration radius, K^+ showed somewhat slower permeation as compared to Na^+.

In Figure 3b, the ionic selectivity of $Ti_3C_2T_x$ and GO membranes is compared. The GO membranes show similar ion selectivity and permeation rates as reported by Joshi.[5] For organic dye cations with hydration radii > 6.4 Å, both permeation rates are on the level of 10^{-4} $mol \cdot h^{-1} \cdot m^{-2}$. However, for small ions (<6.4 Å), GO and $Ti_3C_2T_x$ membranes behave distinctly different, when ion charges are considered. Although single-charged cations showed comparable permeation rates for $Ti_3C_2T_x$ and GO, $Ti_3C_2T_x$ membranes demonstrate significantly lower permeation rates for multiple-charged ions than GO. GO's inability to discriminate between the charges has been reported previously, as arsenate ions (AsO_4^{3-}) permeate through GO membrane at approximately the same rate as single-charged Na^+ or Cl^-,[5] yet GO can sieve out ions larger than 4.5 Å. Thus, $Ti_3C_2T_x$ membranes have a better selectivity than GO membranes for cations of radii <4.5 Å and with charges from +2 to +4, which include alkaline earth ions or pollutant heavy metals, such as Ca^{2+}, Mg^{2+}, Ba^{2+}, Pb^{2+}, Cu^{2+}, Co^{2+}, Ni^{2+}, and Cd^{2+}. This selectivity toward angstrom-sized metal cations with charge dependence is unique when compared with other 2D and porous separation membranes.[5,28−31] Therefore, MXene membranes may be used for water softening and removal of toxic elements. It should be noted that the sieving of cations by $Ti_3C_2T_x$ membranes cannot be attributed to ion adsorption, because the ratio between the mass of feed solute to the membrane exposed (e.g., 1950 mg/g for NaCl vs $Ti_3C_2T_x$) greatly exceeds the adsorption capacity of $Ti_3C_2T_x$ for metal salts (40 to 250 mg/g[15,17−19]).

Cation permeation through $Ti_3C_2T_x$ membranes is greatly affected by their intercalation, which is a size and charge selective process.[20,32] Briefly, single-charged Na^+ or K^+ ions readily intercalate into $Ti_3C_2T_x$ while double-charged Mg^{2+} ions intercalate only after extensive soaking or electrochemical stimulation (applied potential), and bulky ions such as Al^{3+} intercalate only after electrochemical cycling.[20] Thus, the intercalation of large and multiple-charged cations is kinetically hindered. Electrochemical quartz-crystal admittance[21] and atomic force microscopy[22] studies demonstrate that, after the intercalation process, the electrostatic attraction between negatively charged $Ti_3C_2T_x$ and double-charged cations like Mg^{2+} results in a compression of interlayer spacing and shrinkage of the membrane in z-direction.

Based on the obtained results, the permeation rates of cations can be classified into three groups as schematically shown in Figure 4. First, ions that have radii larger than the interlayer distance (~6.4 Å based on XRD) will be excluded outright because they cannot pass through the $Ti_3C_2T_x$ membrane. This is observed in the case of the bulky MB^+ dye cations (permeation rate $\sim 7 \times 10^{-4}$ $mol \cdot h^{-1} \cdot m^{-2}$). In contrast, multiple-charged cations (Mg^{2+}, Ca^{2+} and Al^{3+}) exhibit radii smaller than the interlayer distance, and are able to migrate into the interlayer capillary pathways, which increases the interlayer spacing initially. As more multiple-charged ions intercalate, shrinkage of the layers occurs due to electrostatic attraction between the negatively charged $Ti_3C_2T_x$ surface sheets (Figure SI1) and the highly charged cations, as illustrated in Figure 4b. This shrinkage results in slower permeation rates observed for the multiple-charged ions. Finally, single-charged ions (Na^+) are able to penetrate into the membrane and are attracted to each side of $Ti_3C_2T_x$ layers, forming an electric double layer on the surface of every flake. Adsorption of ions on both sides of MXene, leading to repulsion of MXene sheets, may be accompanied by a slight expansion of the film, which enables higher permeation rates (7−25 times faster than double- and triple-charged ions).

A dead-end filtration setup was used to compare the flux of Na^+, Mg^{2+}, and Al^{3+} chloride solutions through the $Ti_3C_2T_x$ membranes. The membranes were soaked in water or 0.2 mol/L salt solutions for 1 h prior to filtration to ensure saturation

DOI: 10.1021/acs.jpclett.5b01895
J. Phys. Chem. Lett. 2015, 6, 4026−4031

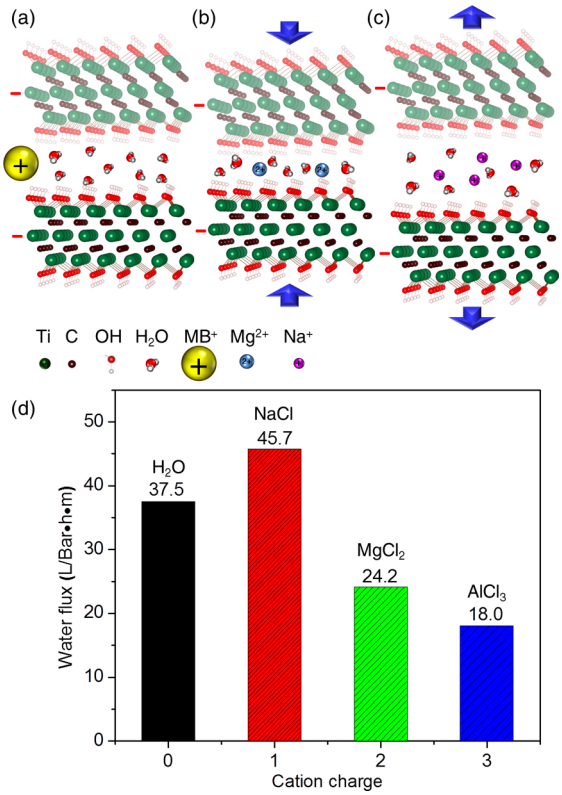

Figure 4. Schematics showing differential permeation of cations through a $Ti_3C_2T_x$ membrane, and total rejection of large MB^+. (a) Cations of radii >6.4 Å cannot penetrate into interlayer spacing. (b) Intercalated smaller multiple-charged cations cause shrinkage of spacing between $Ti_3C_2T_x$ layers, leading to slower permeation. (c) Intercalated small single-charged cations cause expansion of $Ti_3C_2T_x$ interlayer spacing, and they move faster. (d) Water flux of water and salt solutions through the $Ti_3C_2T_x$ membranes as a function of the cation's charge.

equilibrium. The water fluxes of all the solutions decrease in the order NaCl solution > H_2O > $MgCl_2$ solution > $AlCl_3$ solution, as shown in Figure 4d. This trend supports the actuation mechanism for cations permeation, where Na^+ causes membrane expansion and a higher water flux, and Mg^{2+} and Al^{3+} solutions decrease the flux due to contraction of the interlayer spacing. Figure SI3 shows initial results about how intercalated cations in MXene affect water flux of other cation solutions.

The work herein describes a new class of permeation membranes based on $Ti_3C_2T_x$, which are capable of highly selective sieving of cations. This process may be further enhanced through electrical modulation of the surface charge of $Ti_3C_2T_x$ with an applied voltage (electrochemical filtration). If much thinner (e.g., 150−300 nm) supported membranes are used, water flux is expected to increase by at least an order of magnitude. As the 2D MXene family is growing, there is already an array of 17 MXenes (Ti_2C, V_2C, Nb_2C, Nb_4C_3, Mo_2TiC_2 etc.[33,34]), that can be examined as separation membranes. Different surface chemistries, layer thickness, and mechanical properties should allow further tuning of membrane properties. It has been reported that the mechanical strength of $Ti_3C_2T_x$-based membranes can be enhanced by combining $Ti_3C_2T_x$ with polymer poly(vinyl alcohol) (PVA) during membrane fabrication, which may enhance the durability and lifetimes of $Ti_3C_2T_x$-based membranes.[14] Meanwhile, the interlayer spacing could be affected by the addition of different compositional loadings of polymers (PVA or poly(diallyldimethylammonium chloride) (PDDA)). Apart from polymers, layers of CNTs have been demonstrated to open the interlayer spacing of $Ti_3C_2T_x$-based membranes for greater ion fluxes in electrochemical devices.[35] Such hybrid/composite structures may be utilized for high-flux membranes. This proof of concept represents the first study of ion permeability of MXene membranes. Additional systematic studies of fouling and other properties are required in order to evaluate the applicability of different MXenes and select the most promising materials to be used in membranes for ion separation, water purification, desalination, and related applications. The observed differences in transport rates for different ions can also explain the difference in charge−discharge rates of aqueous supercapacitors with different electrolytes[20] and provide guidance in the selection of high-rate electrolytes.

In summary, $Ti_3C_2T_x$ membranes demonstrate attractive separation properties based on their permeation selectivity toward cations of various sizes and charges. The hydrophilic nature of $Ti_3C_2T_x$ accompanied by the presence of H_2O between the layers promotes ultrafast water flux. Besides being nonpermeable to cations with hydration radii larger than the interlayer spacing, $Ti_3C_2T_x$ membranes show high selectivity toward single-, double- and triple-charged metal cations and dye cations of different sizes. $Ti_3C_2T_x$ membranes demonstrate a better performance than GO in the separation of higher charge cations. MXenes, as a new family of 2D materials, may open a door for developing efficient and highly selective separation membranes for ion separation and other technologies.

EXPERIMENTAL METHODS

Preparation of $Ti_3C_2T_x$ Membranes Supported on PVDF. 16.7 mL of $Ti_3C_2T_x$ (0.3 mg/mL) solution was diluted to 500 mL by adding deionized water. The films were fabricated via VAF of the diluted solutions on a PVDF filter membrane (Hydrophilic, 0.45 μm pore size, EMD Millipore Durapore, US) with a diameter of 47 mm. A glass microfiltration apparatus (Feida, China) with a fritted alumina supporting base was used for the VAF. The filtered films were air-dried and kept on the top of the PVDF support.

Preparation of GO Membrane. Purified graphite (SP-1, Carbon Bay) was used to prepare GO via Hummer's method.[36] Dried GO powder was dispersed in deionized water using ultrasonication for 1 h followed by centrifugation at 3500 rpm for 15 min to obtain 1 mg/mL aqueous GO solution. Five milliliters of this solution was diluted to 300 mL with deionized water and underwent VAF in the same way described for $Ti_3C_2T_x$ membranes.

Permeation Tests. The ion permeation experiments were conducted with a homemade U-shaped permeability apparatus shown in Figure SI1. The conductivity of the permeation side was measured by Hanna HI 8633 multirange conductivity meter and recorded as a function of permeation time. Since the permeation was done in wide tubes with a small membrane area, the total water flux was negligible.

Ion Permeation Calculation. The measured ionic conductivity variations of permeate solutions were converted to salt concentrations based on molar conductivity calculations. Molar conductivity is defined as the conductivity of an electrolyte solution divided by the molar concentration of the electrolyte, which is given by $\Lambda_m = (\kappa/c)$, where κ is the

DOI: 10.1021/acs.jpclett.5b01895
J. Phys. Chem. Lett. 2015, 6, 4026−4031

measured conductivity, and c is the electrolyte concentration. Thus, the electrolyte concentration can be obtained as $c = (\kappa/\Lambda_m)$, in which the molar conductivities of all the salt solutions at different concentrations were taken from the literature.[37,38] Then the ion permeation rate, J, was calculated by the classical diffusion equation: $J = V_{eff}c/(A_{eff}t)$, where V_{eff} is the effective volume of the solution on the permeate side; c is the calculated permeation concentration across the membrane; A_{eff} is the effective area of separation membrane; t is the diffusion time. The ion permeability of $Ti_3C_2T_x$ membranes was compared with the values for GO membranes.

Characterization. A scanning electron microscope (SEM, Zeiss Supra 50VP, Germany) was used to study the morphology of the produced flakes and films. The XRD patterns were recorded by a powder diffractometer (Siemens D500, Germany) with Cu Kα radiation at a step of 0.02° and collection time of 0.5 s/step.

Interlayer Distance Calculation. The (0002) peak of the $Ti_3C_2T_x$ membrane shifts from 5.28 to 7.55° after drying. These patterns correspond to a c-Lp of 30.4 Å when wet, 27.0 Å after drying at 70 °C, and 23.4 Å after drying at 140 °C. The c-Lp includes two rigid $Ti_3C_2T_x$ layers plus two interlayer spacings, and one rigid layer of $Ti_3C_2T_x$ has a thickness of 8.8 Å from MD simulations.[9] Thus, the interlayer distance of the 140 °C-dried, 70 °C-dried, and wet $Ti_3C_2T_x$ membranes was calculated to be 2.9, 4.7, and 6.4 Å, respectively.

■ ASSOCIATED CONTENT

Supporting Information

The Supporting Information is available free of charge on the ACS Publications website at DOI: 10.1021/acs.jpclett.5b01895.

Extensive descriptions of the experimental methods and water flux tests (PDF)

■ AUTHOR INFORMATION

Corresponding Authors

*E-mail: kmahmoud@qf.org.qa.
*E-mail: gogotsi@drexel.edu.

Notes

The authors declare no competing financial interest.

■ ACKNOWLEDGMENTS

C.R. and Z.L. were supported by the Chinese Scholarship Council (CSC). K.B.H. was supported by the NSF Graduate Research Fellowship (Grant# 1002809). M.A. was supported by the Libyan North America Scholarship Program (LNASP). SEM and XRD studies were performed at the Centralized Research Facilities (CRF) at Drexel University. The authors thank Michael Ghidiu for XRD analysis, Dr. Babak Anasori for providing Ti_3AlC_2, and Dr. Meng-Qiang Zhao and Prof. Michel Barsoum for useful discussion.

■ REFERENCES

(1) Suk, M. E.; Aluru, N. R. Water Transport through Ultrathin Graphene. *J. Phys. Chem. Lett.* **2010**, *1*, 1590−1594.

(2) Gan, L.-Y.; Zhao, Y.-J.; Huang, D.; Schwingenschlögl, U. First-principles analysis of MoS_2/Ti_2C and MoS_2/Ti_2CY_2 (Y = F and OH) all-2D semiconductor/metal contacts. *Phys. Rev. B: Condens. Matter Mater. Phys.* **2013**, *87*, 245307.

(3) Sun, P.; Zheng, F.; Zhu, M.; Song, Z.; Wang, K.; Zhong, M.; Wu, D.; Little, R. B.; Xu, Z.; Zhu, H. Selective Trans Membrane Transport of Alkali and Alkaline Earth Cations through Graphene Oxide Membranes Based on Cation π Interactions. *ACS Nano* **2014**, *8*, 850−859.

(4) Huang, H.; Ying, Y.; Peng, X. Graphene oxide nanosheet: an emerging star material for novel separation membranes. *J. Mater. Chem. A* **2014**, *2*, 13772.

(5) Joshi, R. K.; Carbone, P.; Wang, F. C.; Kravets, V. G.; Su, Y.; Grigorieva, I. V.; Wu, H. A.; Geim, A. K.; Nair, R. R. Precise and ultrafast molecular sieving through graphene oxide membranes. *Science* **2014**, *343*, 752−754.

(6) Huang, L.; Zhang, M.; Li, C.; Shi, G. Graphene-Based Membranes for Molecular Separation. *J. Phys. Chem. Lett.* **2015**, *6*, 2806−2815.

(7) Sun, P.; Zhu, M.; Wang, K.; Zhong, M.; Wei, J.; Wu, D.; Xu, Z.; Zhu, H. Selective Ion Penetration of Graphene OxideMembranes. *ACS Nano* **2013**, *7*, 428−437.

(8) Naguib, M.; Kurtoglu, M.; Presser, V.; Lu, J.; Niu, J.; Heon, M.; Hultman, L.; Gogotsi, Y.; Barsoum, M. W. Two-dimensional nanocrystals produced by exfoliation of Ti_3AlC_2. *Adv. Mater.* **2011**, *23*, 4248−4253.

(9) Mashtalir, O.; Naguib, M.; Mochalin, V. N.; Dall'Agnese, Y.; Heon, M.; Barsoum, M. W.; Gogotsi, Y. Intercalation and delamination of layered carbides and carbonitrides. *Nat. Commun.* **2013**, *4*, 1716.

(10) Naguib, M.; Mochalin, V. N.; Barsoum, M. W.; Gogotsi, Y. 25th anniversary article: MXenes: a new family of two-dimensional materials. *Adv. Mater.* **2014**, *26*, 992−1005.

(11) Ghidiu, M.; Lukatskaya, M. R.; Zhao, M.-Q.; Gogotsi, Y.; Barsoum, M. W. Conductive two-dimensional titanium carbide clay with high volumetric capacitance. *Nature* **2014**, *516*, 78−81.

(12) Barsoum, M. W. The MAX Phases. In *Nanomaterials Handbook*; Gogotsi, Y., Ed.; CRC Press: Boca Raton, FL, 2006; pp 421−424.

(13) Grimme, S. Semiempirical GGA-type density functional constructed with a long-range dispersion correction. *J. Comput. Chem.* **2006**, *27*, 1787−1799.

(14) Ling, Z.; Ren, C. E.; Zhao, M.-Q.; Yang, J.; Giammarco, J. M.; Qiu, J.; Barsoum, M. W.; Gogotsi, Y. Flexible and conductive MXene films and nanocomposites with high capacitance. *Proc. Natl. Acad. Sci. U. S. A.* **2014**, *111*, 16676−16681.

(15) Ying, Y.; Liu, Y.; Wang, X.; Mao, Y.; Cao, W.; Hu, P.; Peng, X. Two-Dimensional Titanium Carbide for Efficiently Reductive Removal of Highly Toxic Chromium(VI) from Water. *ACS Appl. Mater. Interfaces* **2015**, *7*, 1795−1803.

(16) Dikin, D. A.; Stankovich, S.; Zimney, E. J.; Piner, R. D.; Dommett, G. H.; Evmenenko, G.; Nguyen, S. T.; Ruoff, R. S. Preparation and characterization of graphene oxide paper. *Nature* **2007**, *448*, 457−460.

(17) Mashtalir, O.; Cook, K. M.; Mochalin, V. N.; Crowe, M.; Barsoum, M. W.; Gogotsi, Y. Dye adsorption and decomposition on two-dimensional titanium carbide in aqueous media. *J. Mater. Chem. A* **2014**, *2*, 14334−14338.

(18) Yang, J.-H.; Zhang, S.-Z.; Ji, J.-L.; Wei, S.-H. Adsorption Activities of O, OH, F and Au on Two-dimensional Ti_2C and Ti_3C_2 Surfaces. *Acta Phys.-Chim. Sin.* **2015**, *31*, 0001−0009.

(19) Peng, Q.; Guo, J.; zhang, Q.; Xiang, J.; Liu, B.; Zhou, A.; Liu, R.; Tian, Y. Unique Lead Adsorption Behavior of Activated Hydroxyl Group in Two-Dimensional Titanium Carbide. *J. Am. Chem. Soc.* **2014**, *136*, 4113−4116.

(20) Lukatskaya, M. R.; Mashtalir, O.; Ren, C. E.; Dall'Agnese, Y.; Rozier, P.; Taberna, P. L.; Naguib, M.; Simon, P.; Barsoum, M. W.; Gogotsi, Y. Cation intercalation and high volumetric capacitance of two-dimensional titanium carbide. *Science* **2013**, *341*, 1502−1505.

(21) Levi, M. D.; Lukatskaya, M. R.; Sigalov, S.; Beidaghi, M.; Shpigel, N.; Daikhin, L.; Aurbach, D.; Barsoum, M. W.; Gogotsi, Y. Solving the Capacitive Paradox of 2D MXene using Electrochemical Quartz-Crystal Admittance and In Situ Electronic Conductance Measurements. *Adv. Energy Mater.* **2015**, *5*, 1400815.

(22) Come, J.; Black, J. M.; Lukatskaya, M. R.; Naguib, M.; Beidaghi, M.; Rondinone, A. J.; Kalinin, S. V.; Wesolowski, D. J.; Gogotsi, Y.;

DOI: 10.1021/acs.jpclett.5b01895
J. Phys. Chem. Lett. 2015, 6, 4026−4031

Balke, N. Controlling the actuation properties of MXene paper electrodes upon cation intercalation. *Nano Energy* **2015**, *17*, 27−35.
(23) Han, Y.; Xu, Z.; Gao, C. Ultrathin Graphene Nanofiltration Membrane for Water Purification. *Adv. Funct. Mater.* **2013**, *23*, 3693−3700.
(24) Cicero, G.; Grossman, J. C.; Schwegler, E.; Gygi, F.; Galli, G. Water Confined in Nanotubes and between Graphene Sheets: A First Principle Study. *J. Am. Chem. Soc.* **2008**, *130*, 1871−1878.
(25) Sun, P.; Liu, H.; Wang, K.; Zhong, M.; Wu, D.; Zhu, H. Ultrafast liquid water transport through graphene-based nanochannels measured by isotope labelling. *Chem. Commun.* **2015**, *51*, 3251−3254.
(26) Nightingale, E. R. Phenomenological Theory of Ion Solvation. Effective Radii of Hydrated Ions. *J. Phys. Chem.* **1959**, *63*, 1381−1387.
(27) Fornasiero, F.; Park, H. G.; Holt, J. K.; Stadermann, M.; Grigoropoulos, C. P.; Noy, A.; Bakajin, O. Ion exclusion by sub-2-nm carbon nanotube pores. *Proc. Natl. Acad. Sci. U. S. A.* **2008**, *105*, 17250−17255.
(28) Shannon, M. A.; Bohn, P. W.; Elimelech, M.; Georgiadis, J. G.; Marinas, B. J.; Mayes, A. M. Science and technology for water purification in the coming decades. *Nature* **2008**, *452*, 301−310.
(29) Hinds, B. J.; Chopra, N.; Rantell, T.; Andrews, R.; Gavalas, V.; Bachas, L. G. Aligned multiwalled carbon nanotube membranes. *Science* **2004**, *303*, 62−65.
(30) Surwade, S. P.; Smirnov, S. N.; Vlassiouk, I. V.; Unocic, R. R.; Veith, G. M.; Dai, S.; Mahurin, S. M. Water desalination using nanoporous single-layer graphene. *Nat. Nanotechnol.* **2015**, *10*, 459−464.
(31) O'Hern, S. C.; Boutilier, M. S.; Idrobo, J. C.; Song, Y.; Kong, J.; Laoui, T.; Atieh, M.; Karnik, R. Selective ionic transport through tunable subnanometer pores in single-layer graphene membranes. *Nano Lett.* **2014**, *14*, 1234−1241.
(32) Wang, X.; Shen, Xi; Gao, Y.; Wang, Z.; Yu, L.; Chen, L. Atomic-Scale Recognition of Surface Structure and Intercalation Mechanism of Ti_3C_2X. *J. Am. Chem. Soc.* **2015**, *137*, 2715−2721.
(33) Naguib, M.; Gogotsi, Y. Synthesis of Two-Dimensional Materials by Selective Extraction. *Acc. Chem. Res.* **2015**, *48*, 128−135.
(34) Anasori, B.; Xie, Y.; Beidaghi, M.; Lu, J.; Hosler, B. C.; Hultman, L.; Kent, P. R. C.; Gogotsi, Y.; Barsoum, M. W. Two-Dimensional, Ordered, Double Transition Metals Carbides (MXenes). *ACS Nano* **2015**, DOI: 10.1021/acsnano.5b03591.
(35) Zhao, M.-Q.; Ren, C. E.; Ling, Z.; Lukatskaya, M. R.; Zhang, C.-F.; Van Aken, K. L.; Barsoum, M.; Gogotsi, Y. Flexible MXene/Carbon Nanotube Composite Paper with High Volumetric Capacitance. *Adv. Mater.* **2015**, *27*, 339−345.
(36) Hummers, W. S.; Offeman, R. E. Preparation of Graphitic Oxide. *J. Am. Chem. Soc.* **1958**, *80*, 1339.
(37) Niazi, M. S. K.; Hussain, M. Conductivities and Ionic Association of Copper (11) and Manganese(11) sulfate in water or ethanol. *J. Chem. Eng. Data* **1994**, *39*, 48−49.
(38) Akrawi, B. A.; Ali, A. M. J.; Hani, A. A. M. Study of albumin conductivity in water and its reactions with transition metal ions. *Natl. J. Chem.* **2010**, *40*, 752−769.

DOI: 10.1021/acs.jpclett.5b01895
J. Phys. Chem. Lett. 2015, 6, 4026−4031